Fabrication of flexible composite drug films via foldable linkages using electrohydrodynamic printing

Fabrication of Flexible Composite Drug Films *via* Foldable Linkages Using Electrohydrodynamic Printing

Shuting Wu[a,b], Zeeshan Ahmad[c], Jing-Song Li[a], Ming-Wei Chang [a,b, d*]

[a] Department of Biomedical Engineering, Key Laboratory of Ministry of Education, Zhejiang University, Hangzhou 310027, P.R. China.

[b] Zhejiang Provincial Key Laboratory of Cardio-Cerebral Vascular Detection Technology and Medicinal Effectiveness Appraisal, Zhejiang University, Hangzhou 310027, P.R. China.

[c] Leicester School of Pharmacy, De Montfort University, The Gateway, Leicester, LE1 9BH, UK.

[d] Nanotechnology and Integrated Bioengineering Centre, University of Ulster, Jordanstown Campus, Newtownabbey, BT37 0QB, Northern Ireland, UK.

[*] Corresponding author: Ming-Wei Chang, Ph.D.,

Tel: +44 28 9536 7142, Email: m.chang@ulster.ac.uk

Abstract

The simple method to manufacture a flexible multi-drug with hydrophilic and hydrophobic molecules-loaded composite membrane via three dimensional (3D) electrohydrodynamic (EHD) printing has been demonstrated in this study. The composite membrane consists of two different drug-loaded sections: cellulose acetate-ibuprofen (CA-IBU) and cellulose acetate-paracetamol (CA-Para), respectively, with an intermediate polycaprolactone (PCL) folding component. The composite membranes can be folded and housed in commercial capsules to aid swallowing. By changing the number of PCL layers in the intermediate layers, it is possible to control and modify the mechanical and unfolding properties of the composite membrane. IBU and Para are loaded into the CA polymeric matrix in their amorphous states, with the matrices exhibiting Higuchi and first order release kinetics, respectively. The combination of IBU and Para can potentially be used as analgesic for patients. Magnetic nanoparticles as a functional material can be incorporated into the PCL matrix for wide targeting and traceable applications. The composite membrane here possesses good biocompatibility and flexibility; enabling extensive application prospects in drug combination therapy and personalized medicine.

Keywords: 3D printing; Folding; Drug delivery; Composite.

1. Introduction

Dosage forms administered orally (e.g. tablets, capsules, liquids) are the preferred method of giving medication and are known for patient compliance and safety [1, 2]. Despite this, limitations with respect to controlling drug release and personalizing dosing regimen remain [3]. To circumvent this several strategies have been developed including novel capsule designs (and their manufacturing) which display improved behavior in the gastrointestinal tract [4, 5]. In addition, multi-functional drug delivery devices or technologies are now coming to the fore to address challenges posed for combination therapy (e.g. for cancer and angiocardiopathy [6, 7]. Recent advances have shown that both hydrophilic and hydrophobic drugs can be incorporated in a single dosage and used in synergy to achieve comprehensive therapeutic effects [8].

Three dimensional (3D) electrohydrodynamic (EHD) printing is an ambient environment, non-conventional, one-step process used to prepare 3D microstructures via pre-programmed collector movements [9]. Under optimal applied voltage, the electrified jet undergoes rapid stretching and solidification before reaching the collector. The controlled deposition of fibers is achieved by reducing the distance between nozzle and collector [10]. A variety of materials can be and have been processed to develop pharmaceutical drug carriers via this technique [11]. Compared to other 3D printing techniques (e.g. fused deposition modelling and selective laser sintering), 3D EHD printing provides a processing environment suitable for less thermal stable drugs and the ability to control the process easily and precisely [12, 13]. Moreover, mesh-structure patterning can be used to control surface hydrophobicity and thus drug release [14, 15].

Many polymers such as polyvinyl alcohol (PVA), polycaprolactone (PCL) and cellulose acetate (CA) have been used as drug carrier or matrix materials for drug dosage formulations [16-18]. PCL is a biocompatible polymer with good mechanical properties, which has been applied for various applications requiring strength, such as surgical sutures, wound dressings and filtration [19-21]. Cellulose acetate (CA) is generally prepared through an esterification reaction of cellulose with acetic anhydrides [22]. Due to the biodegradability, hydrophillic nature and excellent stability of CA, it has been widely used for many bio-interfacing applications [23-25], as drug encapsulating matrices, and for drug delivery applications [26].

In recent years, research has been directed towards improving comfort for patients with respect to pain when administrating treatment. Based on this, drug combination therapies have been put forward with the superiority of better analgesic effect when compared to monotherapy [27], whilst improving patient compliance and convenience [28]. Ibuprofen (IBU) is a widely used non-steroidal anti-inflammatory drug (NSAID) with very little side effects, which is used to treat pain and inflammation [29]. Paracetamol (Para) is prescribed as an analgesic and antipyretic with good tolerance and safety [30]. Both IBU and Para are used for pain relief after surgery [31]. It has been proved that the combination of IBU and Para can provide a significantly more effective treatment of acute pain than monotherapies [32].

In this study, we demonstrate the engineering of a flexible multi-drug dosage membrane hosting both hydrophilic and hydrophobic molecules via three dimensional (3D) electrohydrodynamic (EHD) printing. The flexible composite film comprises foldable linkages and the unfolding process enables increased surface area for expedited drug release and increasing retention time which is ideal to reduce dosing. Moreover, loading into different compartments of the composite membrane is a proof-of-concept for combinatorial therapy which is shown via precision 3D printing. The flexible composite membrane with one central component can be folded and enclosed into capsules for oral administration. Composite membranes with different thickness have been fabricated by altering the number of layers of the central components (5, 10 and 20 layers, respectively) to investigate the impacts of the central component layer numbers on the mechanical property and unfolding property of the composite membranes and to find the relatively best parameter. Also, the unfolding process is crucial in terms of expansion potential which is useful for the current application as it can increase the surface area of printed membranes and also prolong retention time in the gastrointestinal tract. IBU and Para were loaded into different regions of the composite membrane and were selected as model drugs to show proof-of-concept for combinatorial therapy and to enable multiple drug release behavior for personalized medicine. Magnetic nanoparticles were added into the central PCL component for potential targeting applications.

2. Materials and Methods

2.1. Materials

Cellulose acetate (CA, M_w = 30000 g/mol), polycaprolactone (PCL, M_w = 80000 g/mol) and ibuprofen (IBU, ≥98%) were all obtained from Sigma-Aldrich, USA. Paracetamol (Para, ≥ 99%) were purchased from Aladdin, China. Acetone, N, N-Dimethylformamide (DMF), acetic acid and phosphate buffer saline (PBS, pH= 7.4) were all obtained from Sinopharm Chemical Reagent, China. Magnetic nanoparticles (Fe_3O_4 NPs) were supplied by HWRK Chem, China. Deionized water (DI water) was prepared in-house (Millipore Milli-Q Reference ultra-pure water purifier, USA). Minimum Eagle's medium (MEM, Gibco) and fetal bovine serum (FBS) were obtained from Invitrogen, USA. All chemicals used were of analytical grade.

2.2. Preparation of 3D EHD printing solutions

Acetone and DMF (acetone:DMF=1:1, v/v) were used to dissolve CA at the concentration of 22% (w/w) by mechanical stirring (VELP ARE heating magnetic stirrer, Italy) for 5 hours. IBU (5% w/w of CA) and Para (4% w/w of CA) were then added to the CA solution, respectively, and dissolved by mechanical stirring for 2 hours to obtain homogenous IBU-loaded CA solution and Para-loaded CA solution. The drug concentration of IBU and Para were altered to demonstrate practical feasibility of personalization and drug loading capabilities for co-therapy.

PCL was dissolved in acetic acid at a concentration of 24 %w/w under mechanical stirring (VELP ARE heating magnetic stirrer, Italy) for 6 hours at room temperature. Fe_3O_4 NPs were added to the PCL solution at a concentration of 0.5 %w/w, which was dispersed through bath sonication for 2 hours to yield a homogeneous suspension.

2.3. Preparation of composite membrane

The 3D EHD printing set-up was shown in Fig. 1, including a stainless steel nozzle (outer diameter = 0.9mm, inner diameters = 0.7 mm), a syringe pump (KD Scientific KDS100, USA), a high voltage power supply (Glassman high voltage Inc. series FC, USA) and a controllable X-Y-Z movement stage. Firstly, the 5 ml syringe was loaded with drug solutions and infused through the printing nozzle at a flow rate of 0.3 ml/h. The path of movement stage was pre-designed and programmed (Adtech, China) in a grid pattern. Under the optimum preparation parameters (applied voltage of 2 kV,

nozzle-to-collector distance of 2 mm and movement stage speed of 100 mm/s), well aligned drug-loaded films with grid shapes were fabricated (6.5 × 13 mm) within 5 min. The layer number of the drug-loaded films were set as 10 layers.

The CA-IBU film and CA-Para film were then linked by the PCL fibrous central component to obtain a flexible, composite membrane. The distance between CA-IBU and CA-Para films was 2 mm. The printing parameters of the central component was optimized to achieve a stable printing Taylor cone. The applied voltage and nozzle-to-collector distance were set to 2 kV and 3 mm, respectively. The flow rate of PCL solution was 0.2 ml/h and the speed of the movement stage was 40 mm/s. The layer number of the central component was set to 5, 10 and 20 layers, respectively (denoted as P5, P10 and P20).

2.4. Mechanical characterization

The mechanical characterization of tension was investigated using a universal material testing machine (Zwick/Roell Z020, Zwick, Germany). The sizes of P5, P10 and P20 were all 13.5 × 15 mm and the thickness of the central components were approximately 40 μm, 70 μm and 140 μm, respectively. Each specimen was fixed by the grips and then tensioned at a rate of 10 mm/min until the composite membranes fractured. Each sample was performed in triplicate.

2.5. Unfolding property test

The unfolding property of the composite membranes was tested in vitro. Each composite membrane was folded and encased in empty capsules (size 0). The composite membrane-loaded capsules were then placed into a 100 ml beaker, containing 60 ml PBS (37 °C). After being left to stand for 15 minutes, the unfolding angles of composite membranes with different folding-part layers were measured using ImageJ software (version 1.48, National Institute of Health, USA). The same test but placed in a HZ-8801K thermostatic oscillator (Taicang Science and Education Factory, China) was also performed and analyzed.

2.6. Fourier transform infrared (FTIR) spectroscopy

The spectra of CA, Para, PCL and the composite membrane were analyzed by Fourier transform infrared spectroscopy (FTIR, IR Affinity 1, Shimadzu, Japan). For each test

disk, 3 mg sample was mixed with 300 mg KBr powders and then pressed into a transparent disk. The disks were then used for FTIR analysis between 400 and 4800 cm^{-1} and the resolution was set as 4 cm^{-1}.

2.7. Differential scanning calorimetry (DSC) and X-ray diffraction (XRD)

Thermal analysis was performed using differential scanning calorimetry (DSC) (PE DSC 7, Perkin-Elmer, USA). Samples (~3 mg) were heated over a temperature range of 30 to 260 °C, at a heating rate of 10 °C/min in the N_2 environment.

XRD analysis of each sample was performed by X-ray crystal diffractometer (Gemini A Ohra, Oxford, UK). The printed membrane was cut into pieces and then sent to XRD test center for analysis. The scan range of 2 theta was between 5 ° and 60 ° at a step size of 0.02 °. The voltage and intensity were 40 kV and 40 mA.

2.8. In vitro drug release

HCl solution (36.46 g/mol) and phosphate buffered saline (PBS, pH=7.4) were used to prepare simulated gastric fluid (SGF, pH=1.7) and simulated intestinal fluid (SIF, pH=7.4), respectively. Drug release tests were performed using a HZ-8801K thermostatic oscillator (Taicang Science and Education Factory, China) at 50 rpm and at the ambient temperature of 37 ±0.5 °C. The tests were first performed in 20 ml SGF for 2 hours and then in 20 ml SIF for 6 hours. The characteristic UV peaks of IBU and Para were 222 nm and 243 nm, respectively (UV-2600 spectrophotometer, Shimadzu, Japan). At time intervals, 3 ml of the release solution was extracted for UV analysis, and then same volume of fresh medium was supplied to the release solution. Each sample was tested in triplicate. The cumulative drug release percentage can be estimated as Equation 1 [18].

$$\text{Drug release } (\%) = \frac{C_t}{C_M} \times 100\% \quad (1)$$

Where C_t is the drug release in the solution at time t and C_M is the total drug release in the solution.

The drug encapsulation efficiency (EE) can be calculated as Equation 2 [33].

$$\text{EE } (\%) = \frac{\text{Amount of drug encapsulated in membranes}}{\text{Theoretical amount of drug}} \times 100\% \quad (2)$$

The drug loading capacity (LC) can be obtained using Equation 3 [34].

$$\text{LC}\ (\%) = \frac{\text{Amount of drug encapsulated in membranes}}{\text{weight of the membrane}} \times 100\% \quad (3)$$

2.9 Kinetics of drug release

The drug release mechanisms of IBU and Para from composite membranes were analyzed by fitting release data to zero-order, first-order, Higuchi and Korsmayer–Peppas mathematic models [14, 35]. The best fit model for drug release can be determined by comparing the correlation coefficient (R^2).

2.10. Scanning electron microscopy (SEM) characterization

Scanning electron microscopy (SEM, Eindhoven, Netherlands) was used to investigate the morphology of the composite membranes. Each Sample was sputter-coated with gold for 90 s before the observation. The accelerating voltage was set as 10 kV. ImageJ software (National Institute of Health, USA) was used to determine the diameters of the printed fibers. The diameter distribution diagrams were obtained by Origin software (version 8.0, Originlab, USA).

2.11. Magnetic test

The magnetic property of the printed composite membrane was investigated using a vibration sample magnetometer (VSM Mini-CFM measurement system, Cryogenic Ltd., UK) at 300 K. Composite membrane with a known weight was placed in the magnetometer and measured in a range of -10000 Oe to 10000 Oe.

2.12. Cell culture

In order to analyze the biocompatibility of the printed composite membrane, L929 mouse fibroblast cells were cultured on the composite membrane with MEM medium containing 1% antibiotic-antimycotic and 10% FBS in a 6 cm diameter culture dish at 37 °C, under 5% CO_2 environment.

After 3 days incubation, cells were fixed with 4 (v/v) % formalin for 30 min and then permeabilized by 0.1% Triton X-100 for 5 min. After being washed three times with PBS, Alexar Fluor 546 phalloidin (1:200 v/v of phalloidin:PBS, Invitrogen, USA) were used to stain the cell cytoskeleton for 20 min followed by triple PBS rinses. 4′, 6′-

diamidino-2-phenylindole hydrochloride (DAPI, 1:5000 v/v of DAPI:PBS, Invitrogen, USA) was then used to stain the cell nuclei for 5 min followed by PBS rinses two times. The cell distribution on the composite membrane was observed by a fluorescent microscope (Nikon Ti-S, Japan).

3. Results and Discussion

3.1. Preparation and characterization of composite membranes

The printed composite membranes and their capsules are shown in Fig. 2. The composite membranes demonstrated grid structure as a result of the pre-determined patterns. The central component (PCL) provides flexability; allowing the composite membrane to fold and thus allowing the composite membranes to be enclosed in size 0 capsules for oral administration. To investigate the effect of the central component layer numbers on mechanical properties and unfolding properties, composite membranes with 5 layers, 10 layers and 20 layers of intermediate PCL component, respectively, were printed and denoted as P5, P10 and P20 accordingly, and the mean weights were measured to be 3.2 ± 0.1, 3.6 ± 0.2 and 4.2 ± 0.1 mg, respectively.

The tensile stress-strain curves of the composite membranes with different folding layers (P5, P10 and P20) are shown in Fig. 3a. It can be seen that the stress-strain curve of P5 was typical for fiber tension exhibiting three characteristic stages including a linear elastic section (region A), a progressive deformation section (region B) and a failure section (region C) [36]. It has been proven that thickness of the fibrous mats affects the its strength [37]. The tensile stress-strain curve of P10 was similar to that of P5 with three characteristic stages. However, here there was a much larger maximum stress due to the increased number of layers of PCL in P10.

The stress-strain curve of P20 showed very different results. An arrow-like pattern with a much smaller elongation was found. During the tension process of P20, the fiber breakage happened on the joint between the drug-loaded sectors and the folding sector, as the insert in Fig. 3a shows.

As shown in Fig. 3b, as the layer number of the central component increased, the

maximum stress of the composite membrane increased from 0.47 ± 0.01 Mpa to 1.52 ± 0.20 MPa, while the maximum strain of the composite membrane decreased from 182 ± 35% to 15 ± 3%. The elastic moduli of P5, P10 and P20 are calculated to be 0.07, 0.36 and 0.72 Mpa, respectively. It is evident that the number of PCL layers plays an important role in the mechanical properties of the composite membranes. The good mechanical property is beneficial for the unfolding property and resisting destruction ability of composite membranes.

To investigate the impact of the central component layer numbers on the unfolding properties, unfolding tests of the composite membranes (P5, P10 and P20) were performed with the unfolding angle data being depicted as shown in Fig. 4. After 15 minutes' standing, the capsule shells dissolved, and the folded composite membranes re-spread out as the inserts of Fig. 4a shows. The unfolding angles of P5, P10 and P20 were calculated to be 44.2 ± 5.8°, 116.0 ± 5.4° and 145.2 ± 2.2°, respectively. This indicates that the unfolding properties of the composite membranes improved with the increase of the central component layer numbers. The results of the similar unfolding test placed in a HZ-8801K thermostatic oscillator for 15 minutes, showed the same varying tendency that the unfolding angles changed from 92.2 ± 7.4° to 148.7 ± 18.3°, as the central component layer number increased from 5 layers to 10 layers. In addition, the unfolding angles of composite membranes with oscillation were larger than those without oscillation, especially P5 which was due to the smaller residual strain and better flexibility. This indicates that oscillation can facilitate the unfolding process of the composite membranes. Taking into consideration of the mechanical properties and unfolding properties as well as the preparation process, P10 was selected as a sample for subsequent studies.

The SEM images of three all 3 sectors in the composite membrane are shown in Fig. 5. Fig. 5a shows the micrograph of the central component with a grid structure. The diameter distribution of the PCL fibers is between 4 μm to 19 μm, and the mean diameter of PCL fibers is 10.5 ± 3.2 μm. Fig. 5a' depicts a detailed image of a PCL fiber, showing the precise stack of the printed PCL fibers with 10 layers. The SEM images of the CA-Para sector and CA-IBU sector of the composite membrane are shown in Figs. 5b and 5c, respectively. It can be seen that both CA-Para matrix and CA-IBU matrix were designed and printed in a grid structure with the grid cell size of

500 × 500 μm^2. The mean diameters of CA-Para fibers and CA-IBU fibers are 15.7 ± 3.6 μm and 18.4 ± 4.8 μm, respectively. As shown in Figs. 5b' and 5c', both printed fibers were well aligned and stacked layer by layer precisely with uniform morphologies. This demonstrates the precision control via 3D EHD printing to manufacture patterned composite membranes.

3.2. FTIR analysis of the composite membrane

To confirm the stability of the compositions and the possible interactions between the materials of the composite membrane, FTIR analysis was performed (Fig. 6). For pure PCL, the characteristic absorption peaks at 2947 cm^{-1} and 1730 cm^{-1} are attributed to the asymmetric stretching of CH_2 and carbonyl stretching, respectively [38]. The absorption peak at 1170 cm^{-1} is related to the stretching of –C-O [39]. These peaks can be identified in the composite membrane spectrum, confirming the presence of PCL in the composite membrane.

For pure CA, the characteristic bands at 3495 cm^{-1}, 1373 cm^{-1} and 1045 cm^{-1} are due to the -O-H group stretching, -C-CH_3 group stretching and –C-O- bond stretching, respectively [40]. For pure IBU, the intense peak at 1720 cm^{-1} is assigned to the carbonyl (C=O) stretching [41], which is overlapping with PCL peak and can be seen in the composite membrane spectrum. The absorption bands at 1230 cm^{-1} and 937 cm^{-1} are due to the stretching of C-C bond and rocking vibration of CH_3 [42], respectively, which, although weak, can be found in the spectrum for composite membrane. For pure Para, the characteristic absorption peaks located at 3319 cm^{-1} and 1554 cm^{-1} are corresponding to –O-H group stretching and N-H group stretching, respectively [27]. All these characteristic peaks appear in the composite membrane spectrum, suggesting the presence of the drugs in the printed composite membrane. Hence, no additional peaks or peak changes were observed in the FTIR spectrum, indicating no physical incompatibilities between the components.

3.3. DSC and XRD analysis of the composite membrane

The DSC curves of pure PCL, CA, Para, IBU and the printed composite membrane are shown in Fig. 7a. An endothermal peak is present at 56.7 °C for pure PCL, indicating the melting point (T_m) of PCL [42]. For pure CA, the first endothermal peak at 67.5 °C and the second peak observed at 230.9 °C correspond to the glass transition temperature

(T_g) of CA, and the melting peak of CA is very close to the its T_g peak around 237 °C [43]. The DSC curve of pure Para shows a well-defined melting peak at 169.2 °C [3]. The sharp endothermic peak located at 77.2 °C corresponds to the melting temperature of pure IBU [44]. For the composite membrane, there are no significant changes in the melting peaks of the polymer PCL and CA, but a slight shift can be identified from 56.7 °C to 51.1 °C for PCL and from 230.9 °C to 222.8 °C for CA. Besides, the endothermal peaks of Para and IBU cannot be seen in the DSC curve of the composite membrane, indicating the amorphous state of both drugs in the printed composite membrane.

The XRD results further confirmed that both drugs were incorporated in the composite membrane in their amorphous forms. As shown in Fig. 7b, the sharp crystalline diffraction peaks of pure Para and IBU were not detectable in the XRD spectrum of the composite membrane because of their dispersion within the matrix material[18]. Although the drug loading was low, it was above the detection limits and can be successfully detected [12, 45, 46].

3.4. In vitro drug release test

The release studies were performed in an acidic medium (gastric pH) for the first two hours then at intestinal pH (PBS) for 6 hours. As seen in Fig. 8, almost 100% of Para was released in the first 2 hours in the gastric medium. In contrast to Para release, IBU release was slower: almost 35% IBU was released during the gastric phase with subsequent sustained release in the intestinal phase. These different release behaviors may be due to the fact that Para is hydrophilic, and IBU is hydrophobic and weak acidic with poor solubility in the acidic media [47, 48]. Fig. 9 shows the SEM images of the three parts of the composite membranes after 8 h drug release test. It can be seen that CA-Para, central and CA-IBU components of composite membrane maintain their grid structures and show no obvious eroding or disintegrating. The magnified images in Figs. 9a', 9b' and 9c' show that the surface morphologies of CA-Para, CA-IBU and central components were all uniform after drug release due to high polymer stability.

The release mechanisms of Para and IBU from the composite membrane was investigated by fitting the release data to zero-order model, first-order model, Higuchi model and Korsmayer–Peppas mathematic model, as shown in Tab. 1. For Para release, it is best fitted by first order model with the highest correlation coefficient $R^2 = 0.9759$ [49]. IBU was best fitted by Higuchi kinetics with R^2 value of 0.9928, indicating the

Fickian diffusion mechanism of IBU, which is further confirmed by Korsmeyer-Peppas modelling with n value of 0.5 [50].

The EE of IBU and Para were calculated to be 85.7 ± 7.2% and 87.9 ± 1.8%, respectively. Maximum EE is not obtained because drug partially diffuses from the semi-liquid polymer on the collector due to evaporation [51]. Moreover, the LC of IBU and Para were calculated to be 2.5 ± 0.3% and 1.3 ± 0.2%, respectively. The results indicate the feasibility of encapsulating drugs via 3D EHD printing.

3.5. Magnetic property

Magnetic nanoparticles (Fe_3O_4 NPs) could be added in the central component, by simply adding them to the printing solution, to further functionalize the composite membranes with magnetic properties. Vibration sample magnetometer (VSM) analysis was performed to quantify the magnetic properties of the composite membrane at a constant temperature (300 K). The hysteresis loop of the printed composite membrane in the field range between -10000 Oe and 10000 Oe is shown in Fig. 10a. The hysteresis loop shows a S-shaped curve with no remanence and coercivity, and the curve goes though the zero point. The saturation magnetization value of the composite membrane is 0.16 emu/g. Therefore, the results manifest the superparamagnetic nature of the printed composite membrane [52]. For better visualization, the magnetic property of the composite membrane was evaluated by a permanent magnet as shown in Fig. 10b. The composite membranes (in distilled water) were drawn to the attracting side by a magnet and was recovered after removal of the magnet. The magnetic composite membranes may have many potential applications such as (but not limited to) magnetic targeting, visualization in MRI and magnetic heating [53, 54].

3.6. Biocompatibility analysis

PCL and CA are FDA approved materials which are widely used in the pharmaceutical industry [55, 56]. However, it is still necessary to investigate the biocompatibility of the composite membranes, due to the potential toxicity of actives and solvents used during the preparation procedures. Herein, L929 cells were cultured on the composite membrane for 3 days. The morphologies of L929 cells were observed through fluorescence microscope as shown in Fig. 11. Figs. 11a, 11b and 11c display the merged fluorescent images of cells growing on the CA-IBU part, CA-Para part and the central

component, respectively. Figs. 11a', 11b' and 11c' are the magnified images of Figs. 11a, 11b and 11c, respectively, showing the detailed cell morphology on the composite membrane. From the inserts of bright field images, it can be seen that cells grew well with the composite membranes, highlighting the good biocompatibility of the composite membranes.

4. Conclusion

In summary, multi-drug-loaded composite membranes consisting of the drug-loaded parts and intermediate folding section were prepared via 3D EHD printing successfully. The composite membrane found to deliver two drugs with well-defined drug release mechanisms. IBU and Para were respectively loaded in two different CA films in their amorphous forms, and linked by the PCL folding layer for the treatmemt of fever or pain alleviation. The mechanical property and unfolding property of the composite membranes were controllable by regulating the layer number of the folding layer. The composite membranes were able to be folded and capsulated into capsules for ease of swallowing, and re-spread out during drug release process. The magnetic property of the composite membrane can be obtained by adding magnetic NPs into the middle PCL layer for targeting applications. The good biocompatibility of the composite membrane was proved via L929 cell culture experiments. These composite membranes were controllable and flexible, and possess potential applications in drug combination therapy and personalized medicine.

Acknowledgements

This research was financially supported by the National Nature Science Foundation of China (No. 81771960), the Fundamental Research Funds for the Central Universities (2017QNA5017) and Key Technologies R&D Program of Zhejiang Province (2015C02035).

Reference

[1] L. Susanne, A.N. Huddleston, Expert Rev. Anticancer Ther., 15 (2015) 1-12.
[2] G.D. Anderson, R.P. Saneto, Adv. Drug Del. Rev., 64 (2012) 911-918.
[3] A. Goyanes, M.P. Robles, A. Buanz, A.W. Basit, S. Gaisford, Int. J. Pharm., 494 (2015) 657-663.
[4] A.M. Bellinger, M. Jafari, T.M. Grant, S. Zhang, H.C. Slater, E.A. Wenger, S. Mo, Y.L. Lee, H. Mazdiyasni, L. Kogan, Sci. Transl. Med., 8 (2011) 365ra157.
[5] J. Liu, Y. Pang, S. Zhang, C. Cleveland, X. Yin, L. Booth, J. Lin, Y.A. Lucy Lee, H. Mazdiyasni, S. Saxton, A.R. Kirtane, T.V. Erlach, J. Rogner, R. Langer, G. Traverso, Nat. Commun., 8 (2017) 124.
[6] Y. Ning, M. Wenzhe, P. Jianfeng, O. Qi, T. Chao, L. Luhua, PLoS One, 9 (2014) 93960.
[7] G.L. Chen, L. Zhang, P. Chen, X.P. Xu, Chin. J. New Drugs, 25 (2016) 2205-2210.
[8] S.A. Khaled, J.C. Burley, M.R. Alexander, J. Yang, C.J. Roberts, J. Control. Release., 217 (2015) 308-314.
[9] Z.-C. Yao, J.-C. Wang, Z. Ahmad, Mat. Sci. Eng. C-Mater., 97 (2019) 776-783.
[10] J.C. Wang, H. Zheng, M.W. Chang, Z. Ahmad, J.S. Li, Sci. Rep., 7 (2017) 43924.
[11] G. Jonathan, A. Karim, Int. J. Pharm., 499 (2016) 376-394.
[12] A. Goyanes, A.B. Buanz, G.B. Hatton, S. Gaisford, A.W. Basit, Eur. J. Pharm. Biopharm., 89 (2015) 157-162.
[13] F. Fina, C.M. Madla, A. Goyanes, J. Zhang, S. Gaisford, A.W. Basit, Int. J. Pharm., 541 (2018).
[14] S. Wu, Z. Ahmad, J.S. Li, M.W. Chang, Mater. Lett., 232 (2018) 134-137.
[15] J.-C. Wang, M.-W. Chang, Z. Ahmad, J.-S. Li, Journal of Drug Delivery Science and Technology, 35 (2016) 114-123.
[16] J. Skowyra, K. Pietrzak, M.A. Alhnan, Eur. J. Pharm. Sci., 68 (2015) 11-17.
[17] A.R. Kirtane, O. Abouzid, D. Minahan, T. Bensel, A.L. Hill, C. Selinger, A. Bershteyn, M. Craig, S.S. Mo, H. Mazdiyasni, C. Cleveland, J. Rogner, Y.L. Lee, L. Booth, F. Javid, S.J. Wu, T. Grant, A.M. Bellinger, B. Nikolic, A. Hayward, L. Wood, P.A. Eckhoff, M.A. Nowak, R. Langer, G. Traverso, Nat. Commun., 9 (2018) 2.
[18] S. Wu, J.-S. Li, J. Mai, M.-W. Chang, Acs. Appl. Mater. Interfaces, 10 (2018) 24876-24885.
[19] H. Yoshimoto, ., Y.M. Shin, H. Terai, ., J.P. Vacanti, Biomaterials, 24 (2003) 2077-2082.
[20] S. Wu, B. Wang, Z. Ahmad, J. Huang, M.W. Chang, J.S. Li, Mater. Lett., 204 (2017) 73-76.
[21] M.A. Woodruff, D.W. Hutmacher, Prog. Polym. Sci., 35 (2010) 1217-1256.
[22] H. Kono, C. Oka, R. Kishimoto, S. Fujita, Carbohyd. Polym., 170 (2017) 23-32.
[23] A. Rajeswari, S. Vismaiya, A. Pius, Chem. Eng. J., 313 (2017) 928-937.
[24] L. Wei, T. Li, G. Li, L. An, L. Fan, Z. Zhang, Carbohyd. Polym., 168 (2017) 153-162.
[25] L. Wu, X. Yin, Z. Guo, Y. Tong, J. Feng, P. York, T. Xiao, M. Chen, J. Gu, J. Zhang, Eur. J. Pharm. Sci., 84 (2016) 132-138.
[26] R. Konwarh, N. Karak, M. Misra, Biotechnol. Adv., 31 (2013) 421-437.
[27] A.P. Chiriac, A. Diaconu, L.E. Nita, N. Tudorachi, L. Mititelutartau, A. Creteanu, O. Dragostin, D. Rusu, G. Popa, Expert. Opin. Drug. Del., 14 (2017) 1.
[28] A. Goyanes, J. Wang, A. Buanz, R. Martínezpacheco, R. Telford, S. Gaisford, A.W. Basit, Mol. Pharm., 12 (2015) 4077-4084.
[29] K.J. Hartlieb, D.P. Ferris, J.M. Holcroft, I. Kandela, C.L. Stern, M.S. Nassar, Y.Y. Botros, J.F. Stoddart, Mol. Pharm., 14 (2017) 1831-1839.

[30] J.C. Mccrae, E.E. Morrison, I.M. Macintyre, J.W. Dear, D.J. Webb, Br. J. Clin. Pharmacol., (2018).
[31] G.E. Kayhana, M. Sanli, U. Ozgul, R. Kirteke, S. Yologlu, J. Clin. Anesth., 50 (2018) 5-11.
[32] S. Daniels, H. Atkinson, I. Stanescu, C. Frampton, Clin. Ther., 40 (2018) 1765-1776.
[33] S. Wu, B. Wang, Z. Ahmad, J. Huang, M.W. Chang, J.S. Li, Materials Letters, 204 (2017) 73-76.
[34] Z.C. Yao, L.J. Jin, Z. Ahmad, H. Jie, M.W. Chang, J.S. Li, International Journal of Pharmaceutics, 524 (2017) 148-158.
[35] S. Gautam, S. Mahaveer, Int. J. Pharm. Studies. Res., 2 (2011) 77-84.
[36] R. Shi, Y. Bin, X. Jian, Polym. Bull., 75 (2017) 1-16.
[37] M. Fadaie, E. Mirzaei, B. Geramizadeh, Z. Asvar, Carbohydr. Polym., (2018).
[38] A.P. Tiwari, M.K. Joshi, J.I. Kim, A.R. Unnithan, J. Lee, C.H. Park, C.S. Kim, J. Colloid Interface Sci., 476 (2016) 29-34.
[39] S.U. Maheshwari, V.K. Samuel, N. Nagiah, Ceram. Int., 40 (2014) 8469-8477.
[40] C. Dumitriu, S.I. Voicu, A. Muhulet, G. Nechifor, S. Popescu, C. Ungureanu, A. Carja, F. Miculescu, R. Trusca, C. Pirvu, Carbohydr. Polym., 181 (2018) 215-223.
[41] L.R. Pires, V. Guarino, M.J. Oliveira, C.C. Ribeiro, M.A. Barbosa, L. Ambrosio, A.P. Pêgo, J. Tissue. Eng. Regen. Med., 10 (2016) 154-166.
[42] C. Karavasili, N. Bouropoulos, I. Kontopoulou, A. Smith, V.D.M. Marisa, I.U.R. Rehman, Z. Ahmad, D.G. Fatouros, J. Biomed. Mater. Res. A., 102 (2014) 2583-2589.
[43] R.R.M.D. Freitas, A.M. Senna, V.R. Botaro, Ind. Crop. Prod., 109 (2017) 452-458.
[44] A.O. Abioye, R. Armitage, A.T. Kola-Mustapha, Pharm. Res., 33 (2016) 337-357.
[45] A. Goyanes, H. Chang, D. Sedough, G.B. Hatton, J. Wang, A. Buanz, S. Gaisford, A.W. Basit, Int. J. Pharm., 496 (2015) 414-420.
[46] T. Tagami, K. Fukushige, E. Ogawa, N. Hayashi, T. Ozeki, Biol. Pharm. Bull., 40 (2017) 357.
[47] S.J. Hwang, G.J. Rhee, K.M. Lee, K.H. Oh, C.K. Kim, Int. J. Pharm., 116 (1995) 125-128.
[48] A. Nabi, S. Tasneem, C.G. Jesudason, V.S. Lee, S.B.M. Zain, J. Mol. Liq., 256 (2018).
[49] S.A. Khaled, J.C. Burley, M.R. Alexander, J. Yang, C.J. Roberts, Int. J. Pharm., 494 (2015) 643-650.
[50] N.A. Peppas, J.J. Sahlin, Int. J. Pharm., 57 (1989) 169-172.
[51] B. Zhang, J. He, X. Li, F. Xu, D. Li, Nanoscale, 8 (2016) 15376.
[52] Y. Gao, M.W. Chang, Z. Ahmad, J.S. Li, Rsc. Adv., 6 (2016) 88157-88167.
[53] M. Arruebo, R. Fernández-Pacheco, M.R. Ibarra, J. Santamaría, Nano Today, 2 (2007) 22-32.
[54] C. Zhang, Y. Li, Y. Hu, Y. Peng, Z. Ahmad, J. Li, M. Chang, ACS applied materials & interfaces, 11 (2019) 7823-7835.
[55] M.N. Nosar, M. Salehi, S. Ghorbani, S.P. Beiranvand, A. Goodarzi, M. Azami, Cellulose, 23 (2016) 3239-3248.
[56] Z.P. Rad, J. Mokhtari, M. Abbasi, Mater. Sci. Eng. C., 93 (2018) 356-366.

Table and Figure Captions

Tables

Table 1. Fitting parameters of Para and IBU release from the composite membrane.

Figures

Figure 1. (a) The schematic of the 3D EHD printing set-up. (b) Image of stable printing cone. (c) The design of the composite membrane, consisting of two drug loaded parts (CA-IBU and CA-Para) and a central component (PCL-Fe_3O_4 NPs).

Figure 2. Photographs of printed composite membranes with different layers of folding part (P5, P10 and P20) with a scale of 10 mm.

Figure 3. (a) Stress-strain curves of different printed composite membranes (P5, P10 and P20), the inserts show the images of P5, P10 and P20 after tension tests with a scale of 10 mm. (b) Maximum stress and Maximum strain of P5, P10 and P20.

Figure 4. The unfolding study of different composite membranes (P5, P10 and P20): (a) unfolding angles and images of P5, P10 and P20 after 15 minutes' standing; (b) unfolding angles and images of P5, P10 and P20 after 15 minutes' oscillation.

Figure 5. SEM images of the composite membrane and the diameter distribution graphs: (a) Central component with 10 layers; (b) CA-Para part with 10 layers; (c) CA-IBU part with 10 layers. (a'), (b') and (c') are magnified images of (a), (b) and (c), respectively.

Figure 6. FTIR spectra of pure PCL, CA, Para, IBU and the composite membrane.

Figure 7. (a) DSC curves of pure PCL, CA, Para, IBU and the composite membrane. (b) XRD patterns of pure PCL, CA, Para, IBU and the composite membrane.

Figure 8. Drug release profiles of Para and IBU from the composite membrane in the simulated gastrointestinal tract.

Figure 9. SEM images of the composite membrane after 8h drug release: (a) central

component; (b) CA-Para part; (c) CA-IBU part. (a'), (b') and (c') are magnified images of (a), (b) and (c), respectively.

Figure 10. (a) Magnetic curves of the composite membrane. (b) Composite membranes response to an externally applied magnetic source.

Figure 11. Fluorescent micrographs of L929 cells with the composite membrane: (a) CA-IBU part; (b) CA-Para part; (c) Central component. (a'), (b') and (c') are magnified images of (a), (b) and (c), respectively. Inserts in (a'), (b') and (c') are bright field images.

Tables

Table 1

Drug	Zero order (R^2)	First order (R^2)	Higuchi (R^2)	Korsmeyer-Peppas (R^2)	n value
Para	0.4407	0.9759	0.7621	-	-
IBU	0.9195	0.9701	0.9928	0.9885	0.5

Figures

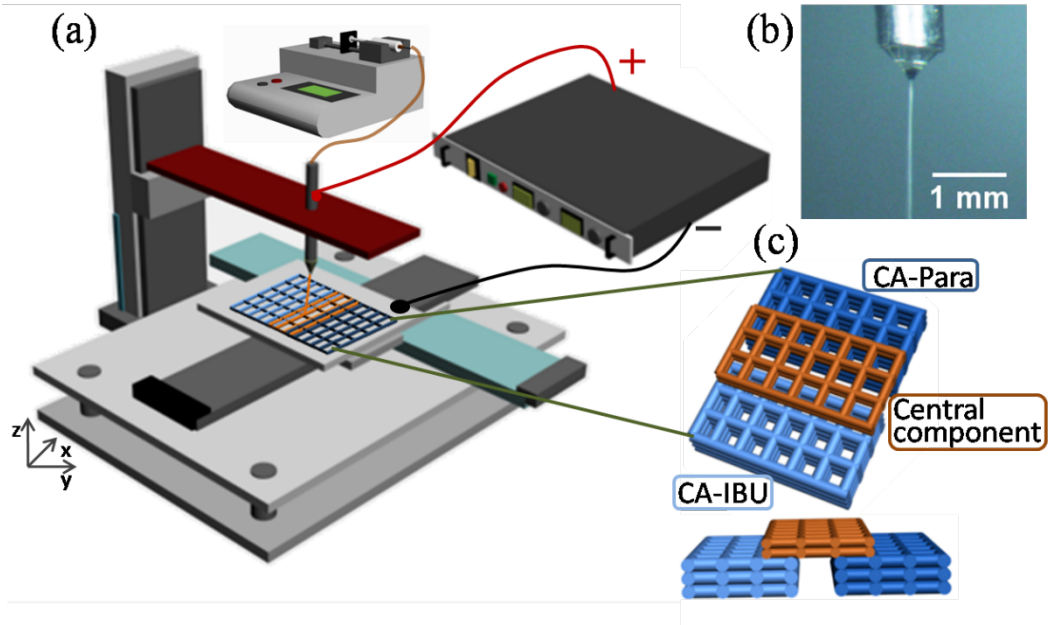

Figure 1

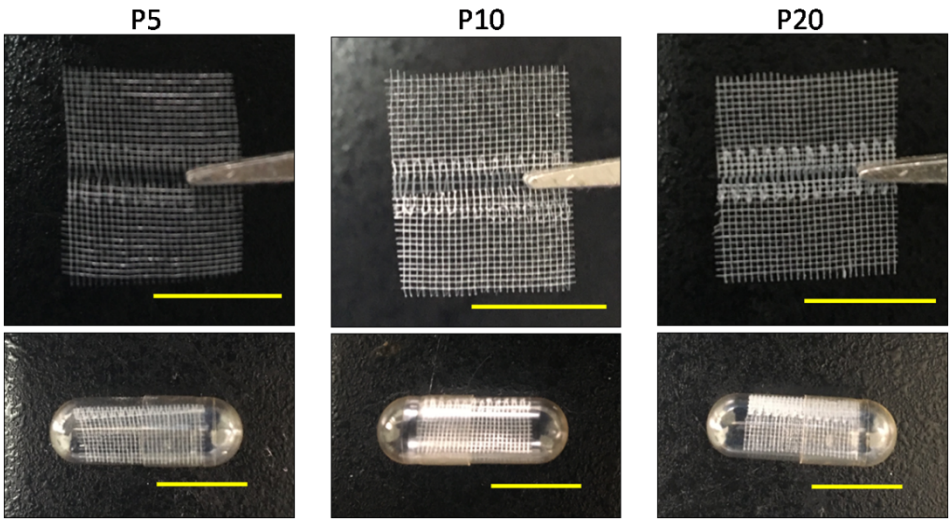

Figure 2

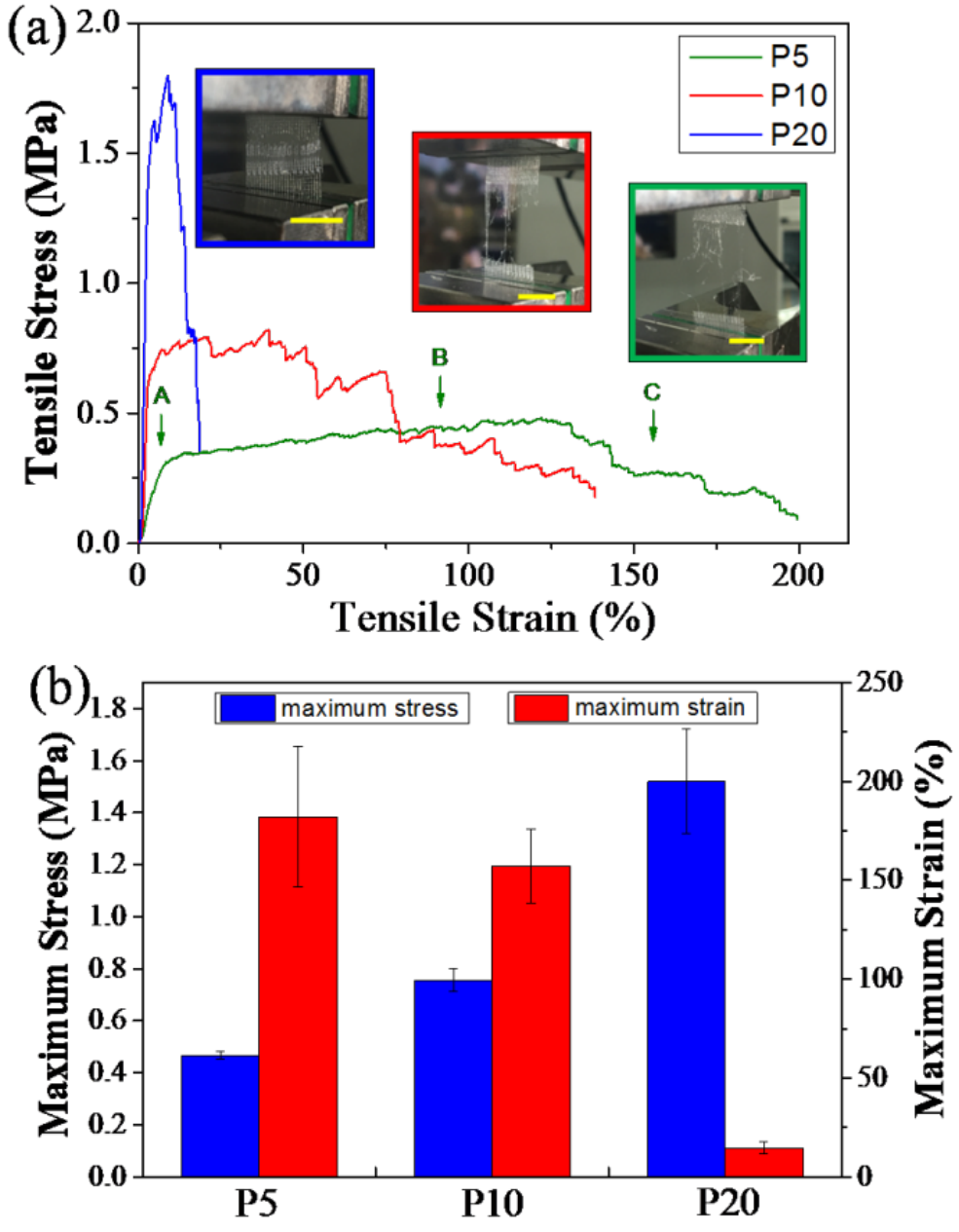
(a)
Tensile Stress (MPa)
Tensile Strain (%)
P5
P10
P20
A
B
C
(b)
maximum stress
maximum strain
Maximum Stress (MPa)
Maximum Strain (%)
P5
P10
P20

Figure 3

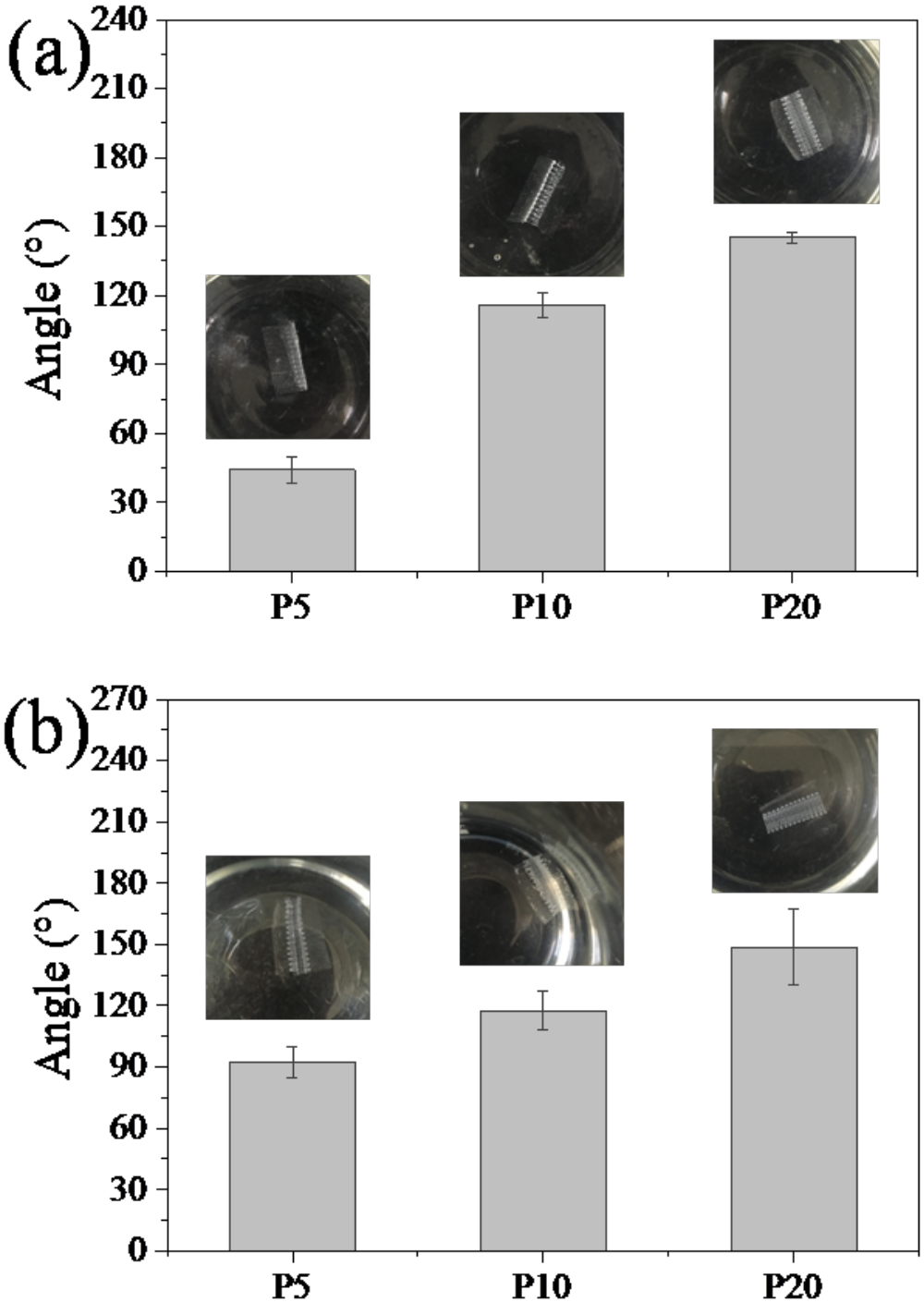
(a)
Angle (°)
240
210
180
150
120
90
60
30
0
P5
P10
P20
(b)
Angle (°)
270
240
210
180
150
120
90
60
30
0
P5
P10
P20

Figure 4

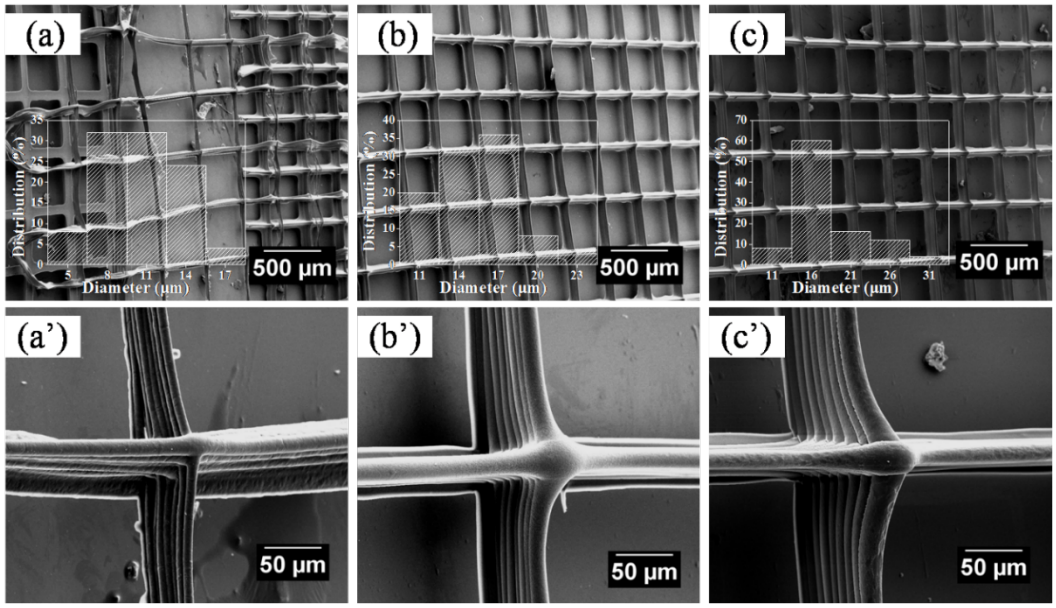

Figure 5

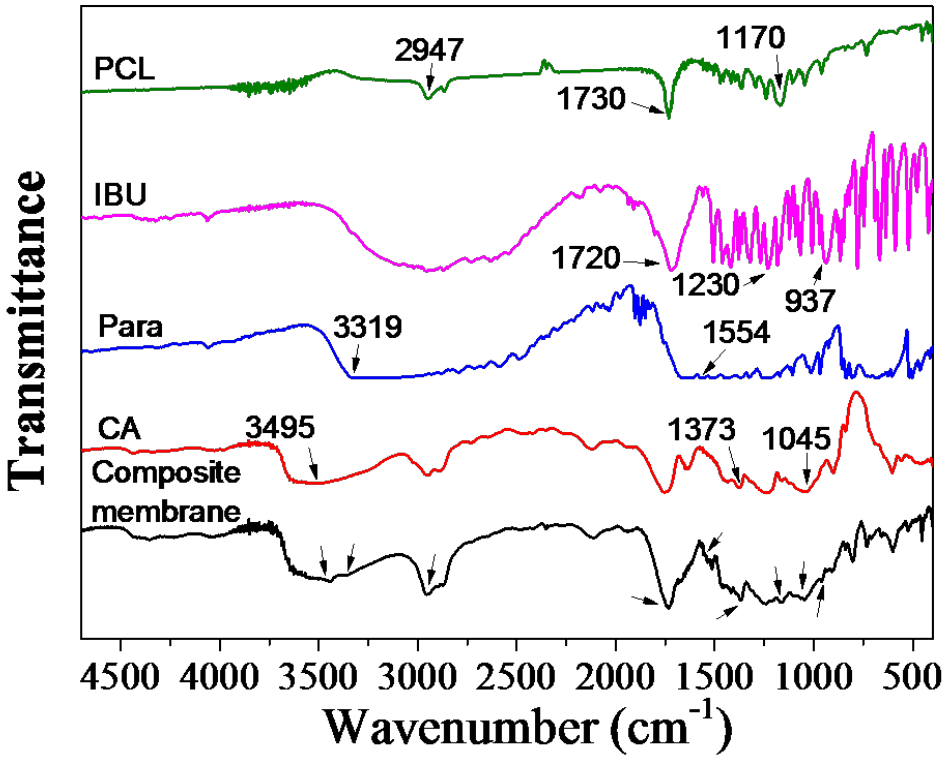
PCL
2947
1730
1170
IBU
1720
1230
937
Para
3319
1554
CA
3495
1373
1045
Composite membrane
Transmittance
4500 4000 3500 3000 2500 2000 1500 1000 500
Wavenumber (cm-1)

Figure 6

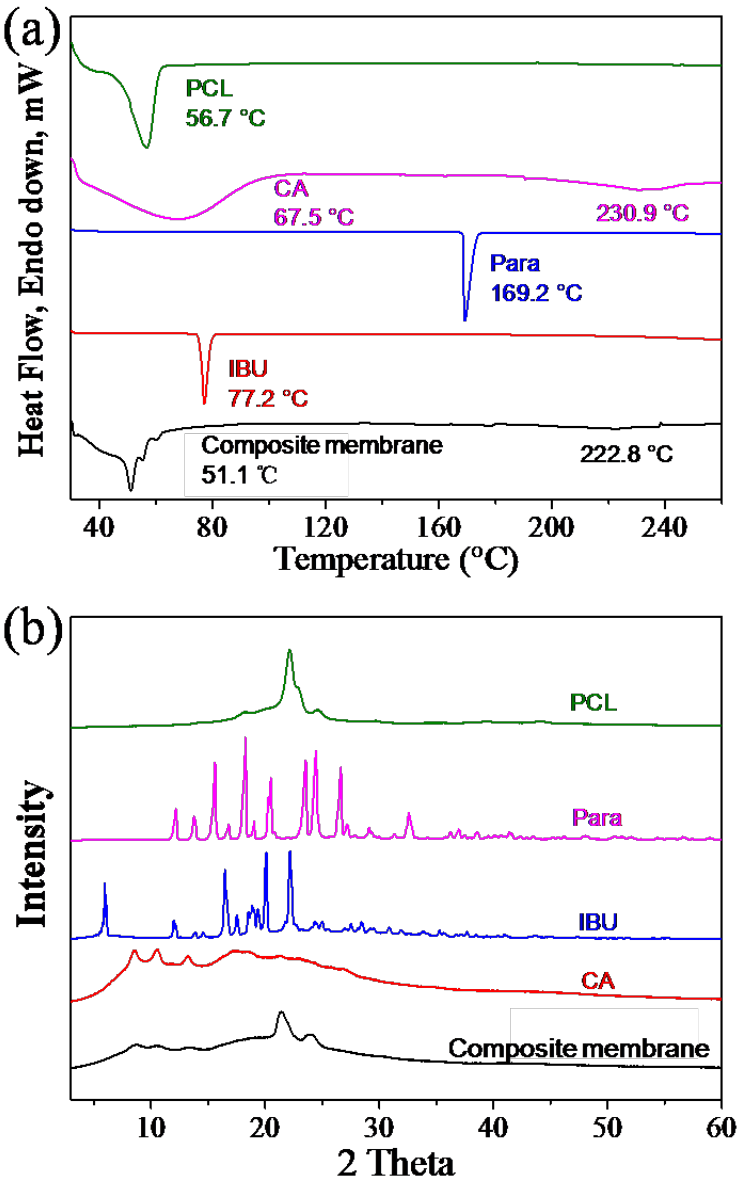
(a)
Heat Flow, Endo down, mW
PCL
56.7 °C
CA
67.5 °C
230.9 °C
Para
169.2 °C
IBU
77.2 °C
Composite membrane
51.1 ℃
222.8 °C
40
80
120
160
200
240
Temperature (°C)
(b)
Intensity
PCL
Para
IBU
CA
Composite membrane
10
20
30
40
50
60
2 Theta

Figure 7

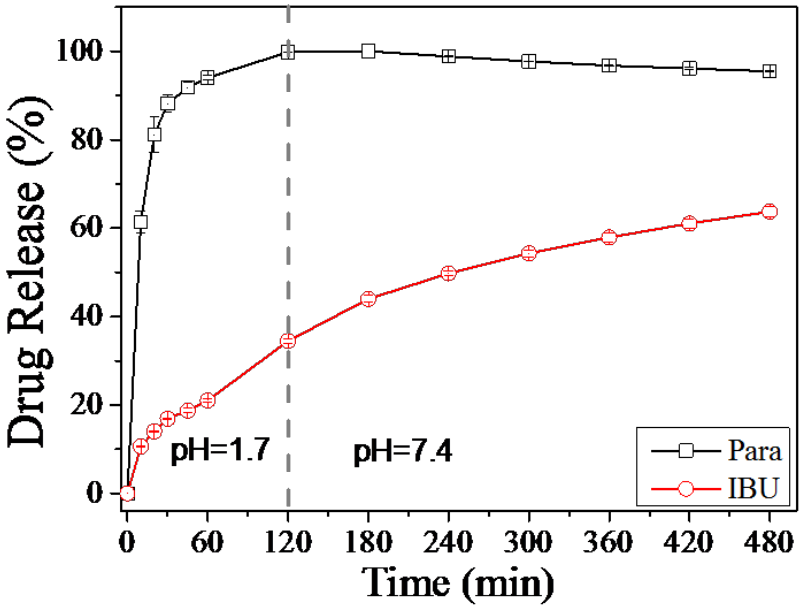
Drug Release (%)
100
80
60
40
20
0
0
60
120
180
240
300
360
420
480
Time (min)
pH=1.7
pH=7.4
Para
IBU

Figure 8

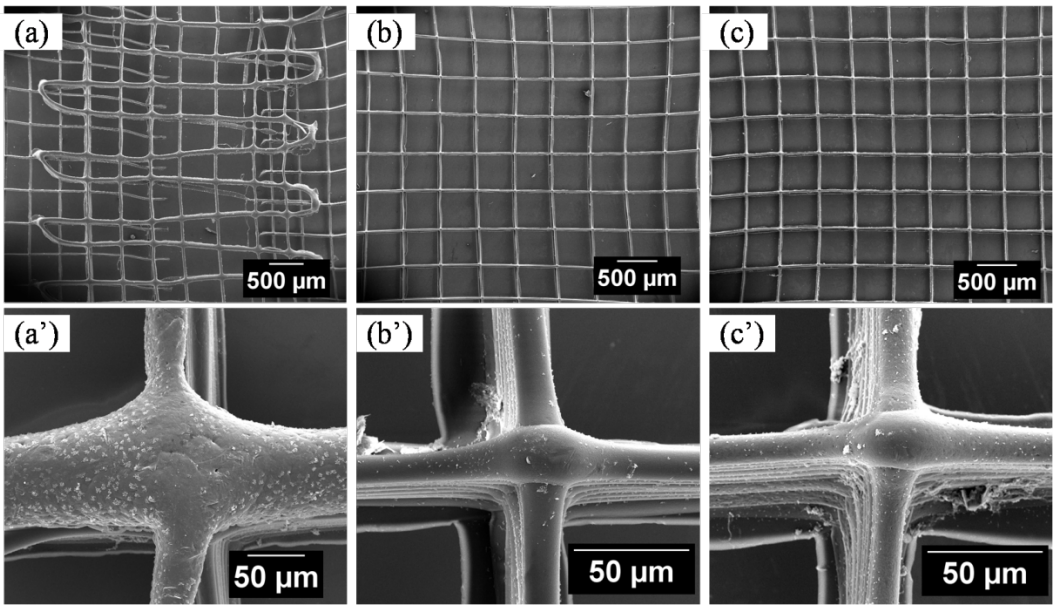

Figure 9

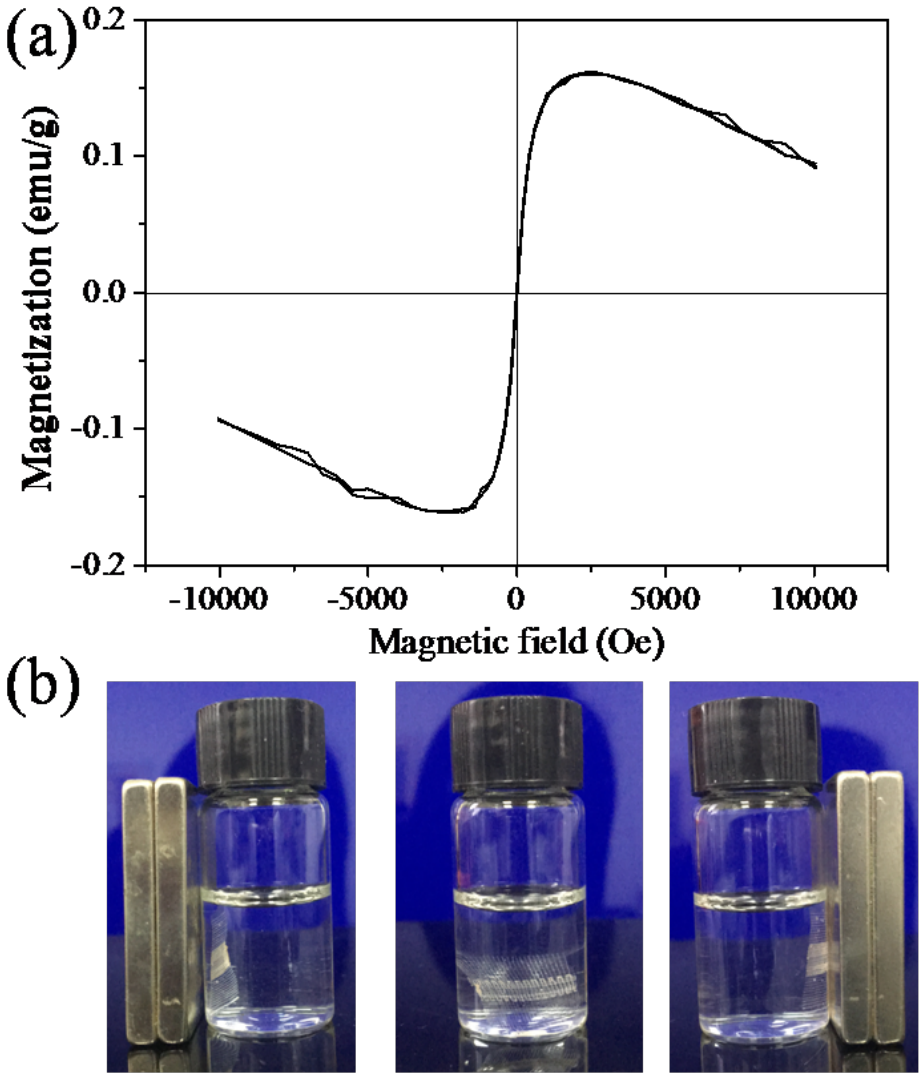
(a)
0.2
0.1
0.0
-0.1
-0.2
Magnetization (emu/g)
-10000
-5000
0
5000
10000
Magnetic field (Oe)
(b)

Figure 10

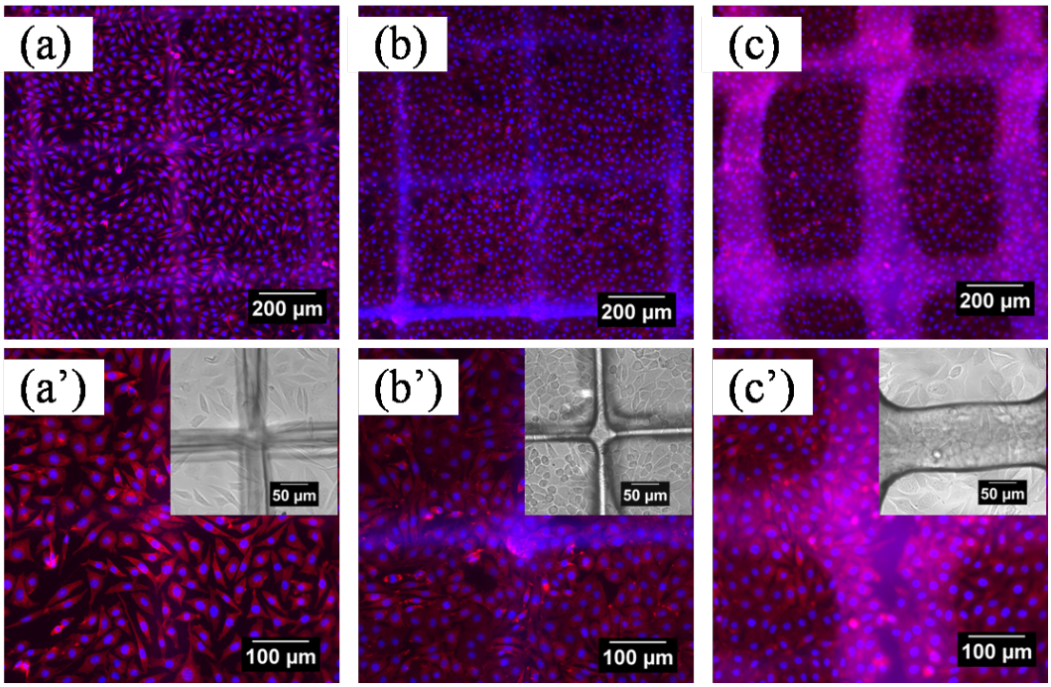

Figure 11